Hindawi Publishing Corporation
Advances in Acoustics and Vibration
Volume 2008, Article ID 574806, 8 pages
doi:10.1155/2008/574806

Research Article

Design and Calibration Tests of an Active Sound Intensity Probe

Thomas Kletschkowski and Delf Sachau

Department of Mechanical Engineering, Faculty of Mechatronics, Helmut-Schmidt-University/University of the Federal Armed Forces Hamburg, Holstenhofweg 85, 22043 Hamburg, Germany

Correspondence should be addressed to Thomas Kletschkowski, kletsch@hsuhh.de

Received 22 November 2007; Revised 4 February 2008; Accepted 13 March 2008

Recommended by Marek Pawelczyk

The paper presents an active sound intensity probe that can be used for sound source localization in standing wave fields. The probe consists of a sound hard tube that is terminated by a loudspeaker and an integrated pair of microphones. The microphones are used to decompose the standing wave field inside the tube into its incident and reflected part. The latter is cancelled by an adaptive controller that calculates proper driving signals for the loudspeaker. If the open end of the actively controlled tube is placed close to a vibrating surface, the radiated sound intensity can be determined by measuring the cross spectral density between the two microphones. A one-dimensional free field can be realized effectively, as first experiments performed on a simplified test bed have shown. Further tests proved that a prototype of the novel sound intensity probe can be calibrated.

1. INTRODUCTION

Noise pollution of enclosed interiors (e.g., aircraft cabins) results in a limitation of human comfort. If noise reduction techniques will be applied in such situations with success, the sound sources at the interior wall that surrounds a standing wave field have to be identified. Especially the localization of low-frequency hot spots in weakly damped enclosures requires the application of advanced measurements techniques. Several noise source localization methods have been established. The methods range from simple sound pressure or sound intensity measurements to more sophisticated methods as beamforming [1] and acoustic holography [2, 3]. A drawback in applying these techniques is that free-field conditions are required. Even though the free field requirement does not have to be met using the inverse boundary element method [4] or the inverse finite element method [5], a well-validated numerical model of the interior is needed, if these techniques will be applied with success.

To avoid the time and cost consuming processes of realizing artificial free-field conditions by introducing passive damping to the interior (which in addition changes the global characteristic of the investigated enclosure) or the need of sophisticated numerical models, a prototype of a new mechatronic sound intensity probe with an active free field (SIAF), see [7], that only influences the local impedance was developed. The fundamental idea is to generate acoustic free-field conditions by active noise control. As shown in Figure 1 (left), the three-dimensional sound field in front of the interior wall is reduced to one dimension by a mechanical device with sound-hard walls. This device is terminated by a loudspeaker. The integrated microphone pair is used to separate the remaining one-dimensional sound field inside the device into its incident and the reflected components. The reflected wave is cancelled by active noise control, as shown in Figure 1 (right). In contrast to common active noise control (ANC) techniques for ducts (e.g., [8, 9]) or common sound tubes with standing wave fields that are used to determine material properties, see [10], the application of the SIAF-approach allows sound intensity measurements in (global) standing wave fields using the local free field of the device.

In a sound field consisting of a free field and a reverberant part, the real part of the time averaged sound intensity determines the free field part. This part vanishes in a purely diffuse, reverberant sound field, and in a plane standing

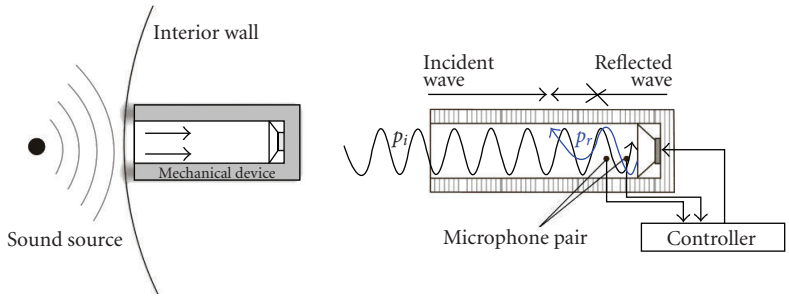

Figure 1: (left) Application and (right) functional principle of an intensity probe with an active free field [6].

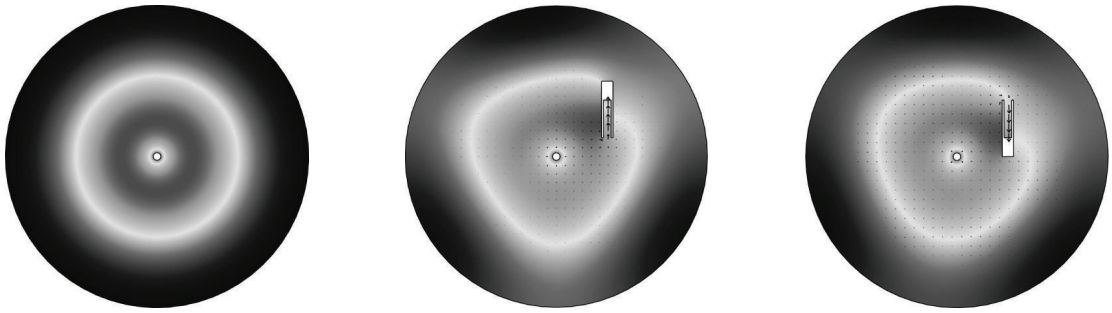

Figure 2: (a) Standing wave field with inactive SIAF and (b) and (c) intensity flow into active SIAF.

wave propagating inside a rigidly terminated enclosure, as shown in [11]. If a spherical wave impinges on the sound soft boundary of a common (passive) sound tube, parts of its energy are reflected in amplitude and phase. In this case, a source is not characterized correctly. A conventional sound tube (without active control) that is placed directly in front of the interior wall would change the impedance of the area of investigation. The resulting impedance could be determined by standard methods, see [10], but this value would vary from point to point. In contrast to this unwanted situation, the SIAF-approach enables both the energy transport from the source into the mechanical device as well as its quantification under comparable boundary conditions inside the mechanical device. Because of the free field inside the probe, the SIAF acts as a local sound absorber. For this reason, the effect of the device on a source would be reduced. A SIAF can therefore be applied for sound source localization, especially in weakly damped interior noise fields at low frequencies. This would—in general—not be possible, if a standing wave field without any energy transport would remain inside the mechanical device. Only the active free field ensures that every acoustic hot spot on the investigated interior wall may radiate into the local free field.

If a SIAF would be used in a standing wave field, but not directly in front of the interior wall, it would still act as a local sound absorber enabling an energy flow into the mechanical device due to active control. This situation is illustrated in Figure 2. Here, the (qualitative) sound pressure distribution as well as the intensity flow (symbolized by black arrows) was determined by two-dimensional time-harmonic ($f = 300\,\text{Hz}$) finite element simulations for an enclosure with sound hard boundaries. The sound source was placed in the center of the cavity. The SIAF is placed top right. The results shown in Figure 2(a) prove that no intensity flow can be measured if the SIAF is inactive. If the inner termination of the SIAF is described by a free-field impedance boundary condition ($Z = 428.75\,\text{kgm}^{-2}\,\text{s}^{-1}$), see Figures 2(b) and 2(c), an energy flow into the mechanical device is enabled. The direction of this energy flow varies with the spatial orientation of the probe, as shown in Figure 2. Therefore, inside the mechanical device it would only be possible to measure the local intensity in longitudinal direction which is—in general—not the magnitude of the intensity vector. Obviously, the localization of a single acoustic hot spot would be impossible, if the SIAF acts as a local absorber in the middle of the sound field. To identify a local source, the SIAF has to be used close to the interior boundary as shown in Figure 1 (left). The minimum working distance should be chosen in such a way that contact between the SIAF and the interior wall is excluded. The maximum working distance has to be small enough to ensure that an energy flow into the SIAF results only from a source that is located on the investigated part of the boundary. Assuming an upper frequency limit of 1kHz, due to the area of application of ANC, the maximum working distance should be lower than ten percent of the minimum wave length (e.g., 3 cm).

This paper is divided into four parts. The first explains the calculation of the reflected wave and the control concept. Furthermore, experimental results of tests that were performed on a simplified test bed are reported. The second part

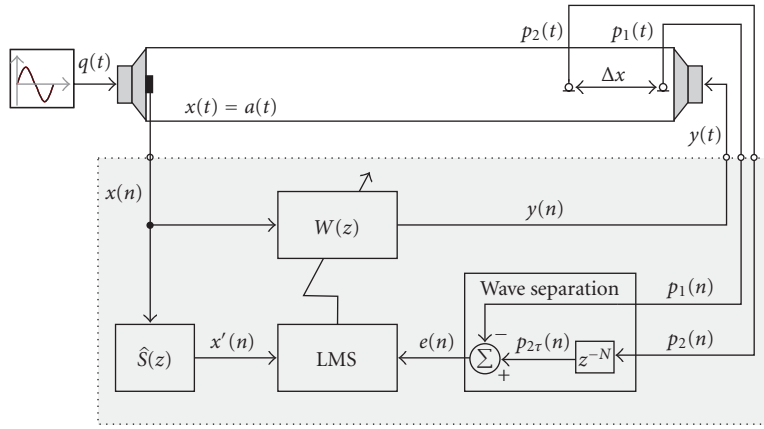

Figure 3: Block-diagram for SIAF-approach based on wave separation in time domain.

presents the results of calibration tests that were performed on a SIAF-prototype. A short summary is given in the third part of the paper.

2. CONTROL STRATEGY AND PROOF OF CONCEPT

To realize free-field conditions, the sound field inside the mechanical device has to be separated into its incident and reflected components. This separation can be performed in frequency as well as in time domain. As wave separation in frequency domain requires a frequency domain control algorithm, it was not applied. Instead, a time domain approach was used for time-discrete adaptive control, as illustrated in Figure 3.

As shown in [12], the reflected wave component of a one-dimensional standing wave field can be determined by employing two microphones and a time-delay. One of the SIAF microphones has to be placed in front of the canceling loudspeaker at $x = 0$, the other at a distance Δx. Assuming plane wave propagation, the total pressure at the discrete time step n picked up at the microphones is given by

$$\begin{aligned} p_1(n) &= p_i(0,n) + p_r(0,n), \\ p_2(n) &= p_i(\Delta x, n) + p_r(\Delta x, n) \\ &= p_i(0, n+N) + p_r(0, n-N), \end{aligned} \tag{1}$$

where the continuous time delay $\tau = T_s N = \Delta x/c$ is given by the separation distance Δx, the sample time T_s, the number of delayed time steps N, and the speed of sound c. If $p_2(n)$ is delayed by τ, the delayed sound pressure is defined as

$$p_{2\tau}(n) = p_2(n-N) = p_i(0,n) + p_r(0, n-2N), \tag{2}$$

and the error signal $e(n)$ that is calculated as follows

$$e(n) = p_{2\tau}(n) - p_1(n) = p_r(0, n-2N) - p_r(0,n) \tag{3}$$

represents the reflected wave only. As shown in [12], the calculation of the error signal fails, if the distance between the microphones equals a multiple of one half of the wave length, if (3) is analyzed for tonal excitation $p_r(0,n) = A\sin[2\pi f(nT_s - x/c)]$. As shown in [6], the time delay number N is limited by Shannon's law $1 \leq N < T_{\min}/2T_S$, there $T_{\min}$ represents the periodic time of the highest frequency of interest $f_{\max}$.

As shown in Figure 3, the filtered reference least mean square (FxLMS) algorithm was used to update the coefficients of the adaptive finite impulse response (FIR) filter $W(z)$. These coefficients are used to generate the driving signal $y(n)$ for the canceling loudspeaker. The acceleration of the interior wall that in the simplest case is represented by the membrane on the noise source was used as reference signal $x(n)$ that is required for adaptive feed foreword control. A feedback controller would be independent of a reference signal. But, in contrast to an adaptive control scheme based on FIR filters, a feedback controller based on infinite impulse response (IIR) filters is not unconditionally stable, see [13]. Offline plant modeling based on the common least mean square algorithm was applied to identify the secondary path model $\hat{S}(z)$. As shown in [13], the single-channel leaky FxLMS algorithm can be summarized as follows.

(1) Adaptive filtering

$$y(n) = \mathbf{w}^T(n)\mathbf{x}(n), \tag{4}$$

where $y(n)$ is the controller output at the discrete time step n, $\mathbf{w}(n)$ is the $L \times 1$ column matrix of the filter coefficients for a FIR filter of length L, and $\mathbf{x}(n)$ is the $L \times 1$ column matrix of the buffered reference signal $\mathbf{x}(n)$.

(2) Single-channel prefiltering

$$\mathbf{x}'(n) = \sum_{i=0}^{I-1} \hat{s}_i(n)\mathbf{x}(n-i), \tag{5}$$

where I is the order of the FIR filter $\hat{S}(z)$.

(3) Weight vector update

$$\mathbf{w}(n+1) = \nu\mathbf{w}(n) + \mu\mathbf{x}'(n)e(n), \tag{6}$$

where ν is the leakage factor, μ is the convergence factor, and $e(n)$ is the error signal at the discrete time step n.

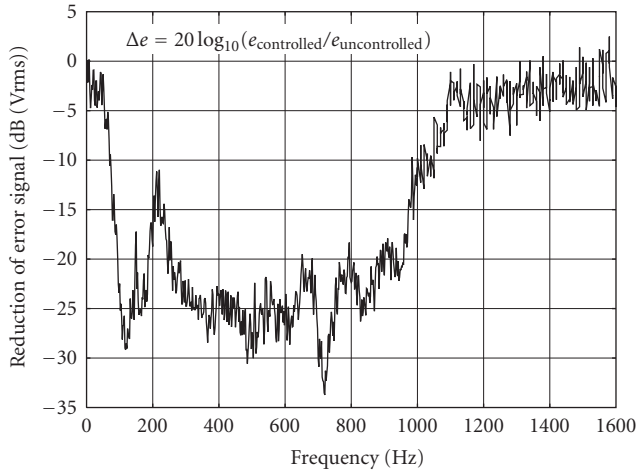

Figure 4: Broadband noise reduction obtained by SIAF approach applied to a sound tube.

The choice of a proper filter length L depends on parameters such as the characteristics of the error signal (e.g., tonal or broadband), the impulse response of the secondary path, and the computing power of the applied signal processor. For tonal excitation, a filter length of $L = 2$ would be sufficient to determine amplitude and phase of the control signal as well as to model the secondary path. In practice, however, a filter length of $L = 4$ can be advantageous, because of the nonideal transfer behavior of many electro-dynamic loudspeakers at very low frequencies. If broadband disturbances have to be controlled using a certain sampling frequency, the number of filter taps must be high enough to model the impulse response of the secondary path in the analyzed frequency band but small enough to guarantee causality.

To test the performance of the SIAF approach, the algorithm was implemented on a real time processor (type: dSpace DS1103). The time delay number was set to $N = 2$. As motivated by Figure 3, a sound tube with a square cross-section (edge length $a = 92$ mm) and upper frequency limit $f_u \approx 1864$ Hz (according to [10, equation (2)]) terminated by electro-dynamical loudspeakers (type: SPEAKA MT 60/80) was used as a simplified test bed for first experiments. Two microphones (type: Ono Sokki MI-1233) were used. Microphone 1 was placed in front of the canceling loudspeaker and microphone 2 in a distance of $\Delta x = 13.7$ cm. In compliance with [10, equation (4)], the upper frequency limit was reduced to $f_{\text{ured}} \approx 1152$ Hz for this reason. An accelerometer (type: B&K 4374) that was amplified by a signal conditioner (type: B&K Nexus 2692) was used to detect the reference signal. Furthermore, several analogue high- and low-pass filters, respectively, (type: Kemo VBF21) were applied to avoid aliasing. A multichannel FFT analyzer (type: Ono Sokki DS2100) was used for data analysis.

The reduction of the reflected waves was analyzed for a broadband disturbance with $f_{\max} < f_{\text{ured}}$. The system was excited by frequency-banded white noise ($50\,\text{Hz} \leq f \leq 1\,\text{KHz}$). Therefore, a filter length of $L = 128$ was used for the adaptive weight vector $\mathbf{w}(n)$ as well as for the secondary path model $\hat{S}(z)$. The sampling frequency was set to $f_S = 5$ kHz. The results shown in Figure 4 prove that the controller cancels a reflected wave, if and only if the associated frequency is detected by the reference sensor. A total reduction of -16.2 dB was achieved in the analyzed frequency band. The SIAF-control-strategy was applied successfully. Sound intensity was not determined during this test.

3. DESIGN OF A PROTOTYPE AND CALIBRATION TESTS

A first realization of a SIAF that is based on commercial components is shown in Figure 5(a). It consists of a sound source (type: B&K 4295) and a self-made cylindrical adapter (inner diameter $d = 38$ mm). Two phase-matched microphones (type: B&K 4295) were integrated into this adapter. A portable FFT analyzer (type: B&K 3560B with a phase match of $\pm 0.017°$ at 50 Hz using B&K sound intensity probes) was used for data processing. The microphone spacing was set to $\Delta x = 10$ cm. According to [10, equation (4)], the upper frequency is given by $f_{\text{ured}}^{\text{SIAF}} \approx 1543$ Hz.

An anechoic chamber was used to test the possibility of calibrating the SIAF prototype. The experimental setup is shown in Figure 5(b). An electro-dynamical loudspeaker (type: PAB-8MK2) was used as the acoustic source, and a free-field microphone (type: B&K 4188) was applied to measure the sound pressure level at a fixed reference point. An accelerometer (type: B&K 4374), amplified by a signal conditioner (type: B&K Nexus 2692), was used to assure a precise reproduction of the excitation and to detect the reference signal. The radiated sound intensity was measured for the third-octave band center frequencies between 80 Hz and 500 Hz. First reference data were collected by a conventional sound intensity probe (type: B&K 3595 with microphone pair 4197 using a spacer of 12 mm). The measurements were then repeated using the SIAF prototype. Signal processing was performed on a power computer (type: dSpace DS1103). Tonal disturbances were used to test the SIAF prototype. Therefore, a filter length of $L = 4$ was used for the adaptive weight vector $\mathbf{w}(n)$ as well as for the secondary path model $\hat{S}(z)$ which was remodeled for every frequency. The time delay number was set to $N = 2$, and a sampling rate of $f_S = 10$ kHz was used for these tests.

The results shown in Figure 6(b) prove that the controller was capable of reducing the reflected wave for all analyzed frequencies. Only minor sound pressure deviations between the SIAF microphones were measured. The results presented in Figure 6(b) also confirm sound propagation in a plane wave field, because the same amount of energy was determined at the two measurement points. For this reason and because of the fact that the distance between the loudspeaker membrane and the front side microphone of the SIAF was smaller than the triple diameter of the tube, compare with [10], additional corrections for the losses along the boundaries of the tube (needed for higher frequencies, $f > 500$ Hz) were not taken into account.

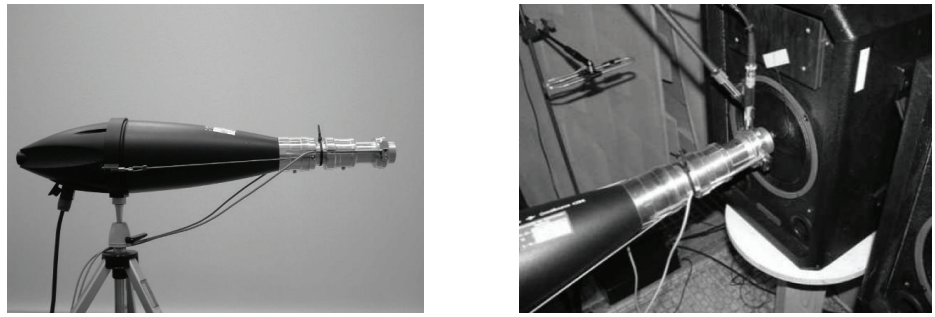

(a) (b)

Figure 5: (a) SIAF prototype, see [6], and (b) experimental setup for calibration tests.

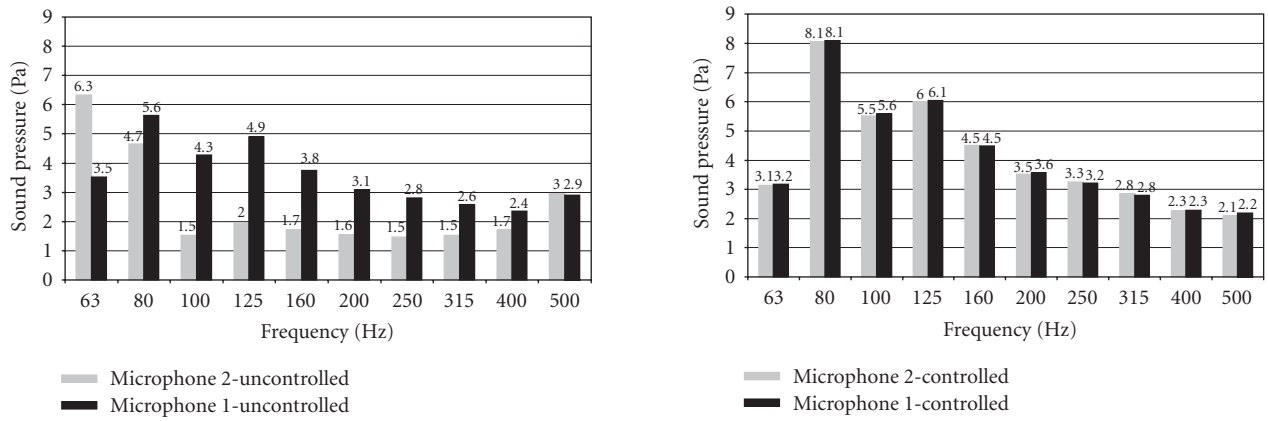

(a) (b)

Figure 6: Sound pressure at the SIAF microphones: (a) uncontrolled and (b) controlled.

As proposed in [11], the sound intensity was calculated from the imaginary part of the cross-spectral density $G_{12}(f)$ between the two SIAF microphones (p-p probe):

$$I(f) = -\frac{1}{2\pi f \rho \Delta x} \mathrm{Im}[G_{12}(f)], \tag{7}$$

where ρ is the density of the fluid. An alternative approach is given by the application of the combined sound-pressure, particle-velocity probe (p-u probe) that is described in [14]. This probe consists of a small electret condenser microphone and a particle velocity transducer. The latter is based on the technique of the acoustic intensity meter that was proposed in [15]. Particle velocity measurements using transducers that were analyzed in [16] were only possible by using a small fan to generate a permanent air flow. Because of the nonlinearities of these transducer types, the permanent air flow is needed to define the working point of the sensor. The p-u probe, presented in [14], is independent of a permanent air flow, and its application, especially in plane standing wave fields, ensures that at least one of the transducers is not located at a nodal point. If, however, the sound pressure level exceeds the upper sound level—110 dB, see [17]—of the electret microphone, the pressure sensor of the p-u probe can cause nonlinearities, as shown in [18]. This operating mode must be avoided, if a linear controller is applied. As shown in [14], the application of a p-u probe is advantageous, if the influence of background noise—coming from sources outside the measurement plane—on the phase mismatch between the sensors has to be reduced. In contrast to the phase mismatch between the two microphones of a p-p probe, the p-u phase mismatch is exacerbated in strongly reactive sound fields (e.g., in a plane standing wave), see [14]. Furthermore, it is more difficult to calibrate a p-u probe than a p-p probe, as concluded in [14].

The SIAF approach requires a wave separation in the time domain that is based on two microphones. Therefore, sound intensity measurement was performed according to (7). This procedure enables a direct comparison between the sound intensity that is measured using the SIAF approach and the sound intensity that is determined by a conventional p-p probe. The measurement limitations of this approach for sound intensity measurement are summarized in [11]. Neglecting errors coming from off-axis measurements, the quality of the results is determined by the phase mismatch error, the finite difference approximation error, and the near field error.

The phase mismatch between the two channels in the analyzing system determines the "low-frequency limit," see [11]. As written in [11], the maximum phase mismatch might be $\pm 0.3^\circ$ for a good probe and analyzer combination.

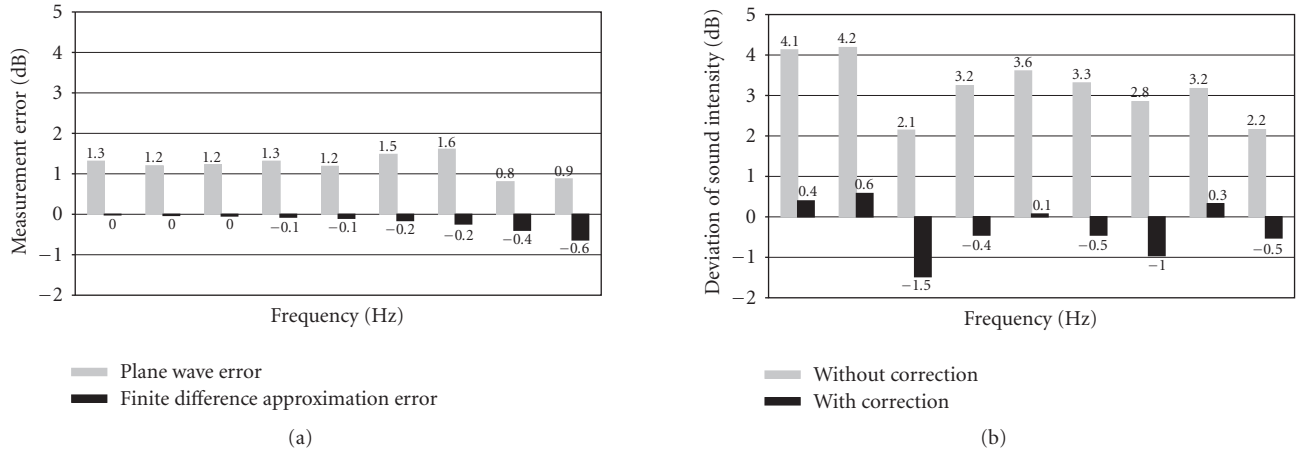

Figure 7: Effect of errors (a) on sound intensity measurement and (b) deviation in sound intensity.

The calibration tests were performed using phase matched microphone-analyzer combinations. In this case, the phase mismatch at low frequencies depends only on the microphone spacing. Using a 12 mm spacer for the conventional sound intensity probe and a spacing of 10 cm for the SIAF, the change of phase over the spacer is given by $\pm 1^\circ$ and $\pm 8.4^\circ$ for the SIAF and for the lowest analyzed frequency, respectively. Hence, phase mismatch errors were not taken into account during the calibration tests. If the SIAF concept is applied using a microphone-analyzer combination that is not perfectly calibrated in phase, phase calibration (e.g., by a procedure based on switching the microphones as described in [10]) is required. As also outlined in [11], the finite difference approximation error of an ideal two-microphone sound intensity probe in a plane wave of axial incidence is given by

$$E_{\mathrm{FD}}(f) = 10\log_{10}\frac{\sin k\Delta x}{k\Delta x}, \quad \text{with } k = \frac{2\pi f}{c}. \tag{8}$$

This error determines the "high-frequency limit" of a *p-p* probe. It has to be taken into account that, because the pressure gradient that is needed to calculate the particle velocity is approximated by a simple finite difference scheme every time, the intensity is measured. If a *p-u* probe is used for sound intensity measurements, E_{FD} can be avoided, because the particle velocity is measured directly. A finite difference approximation of the pressure gradient is not needed in this case. The "high-frequency limit" as well as the "low-frequency limit" of a *p-u* probe is determined by the frequency response curves of the microphone and the particle-velocity transducer.

Using the calculations for a two microphone probe in a sound field of a point source radiating into a free field, as presented in [11], the near field error can be described as follows:

$$E_{\mathrm{NF}}\left(\frac{\Delta x}{x}\right) = -10\log_{10}\left(1 - \frac{1}{4}\left(\frac{\Delta x}{x}\right)^2\right). \tag{9}$$

The near field error described by (9) is a function of the separation distance between the two microphones Δx and the distance from the source to the middle point between the microphones x. A negligible near field error of 0.063 dB was determined for the conventional sound intensity probe with the 12 mm spacer ($\Delta x = 1.2$ cm, $x = 5$ cm), but it was found that an overestimation of $E_{\mathrm{NF}} = 2.4$ dB has to be taken into account for a SIAF ($\Delta x = 10$ cm, $x = 7.6$ cm) without a surrounding tube.

In addition to these measurement limitations, and because of the tube that surrounds the SIAF-microphone pair, the deviations between plane wave propagation in one dimension inside the SIAF and spherical wave propagation in three dimensions have to be taken into account by RMS values of the measured sound pressure:

$$E_{\mathrm{PW}}(f) = 20\log_{10}\left(\frac{\tilde{p}_2}{2\cdot 10^{-5}\,\mathrm{Pa}}\right) - 20\log_{10}\left(\frac{\tilde{p}_{\mathrm{Ref}}}{2\cdot 10^{-5}\,\mathrm{Pa}}\right). \tag{10}$$

This error is in the following called plane wave error. It was calculated as the difference between the sound pressure level measured at SIAF-microphone 2 and the sound pressure level measured at the reference microphone. The latter was placed above the actively controlled SIAF, as shown in Figure 5(b).

The frequency dependencies of the plane wave error (that was derived from measurements) as well as of the finite difference approximation error, given by (8), are shown in Figure 7(a). It can be seen that the first results in an overestimation of the measured sound pressure level. The second leads to an underestimation of the measured sound intensity level.

The deviation $\Delta I = I_{\mathrm{SIAF}} - I_{\mathrm{Conv}}$ between the sound intensity that was measured using the SIAF prototype and the sound intensity that was determined by the conventional probe is shown in Figure 7(b). It was found that these deviations can be reduced, if (a) the near field error, (b) the finite difference approximation error, and (c) the plane wave error are used to calculate a corrected deviation $\Delta I_{\mathrm{corr}} = \Delta I - (E_{\mathrm{FD}} + E_{\mathrm{NF}} + E_{\mathrm{PW}})$. The corrected values are also shown in Figure 7(b). Without correction, the measurement error was at least 2.1 dB. Using the correction based on the three

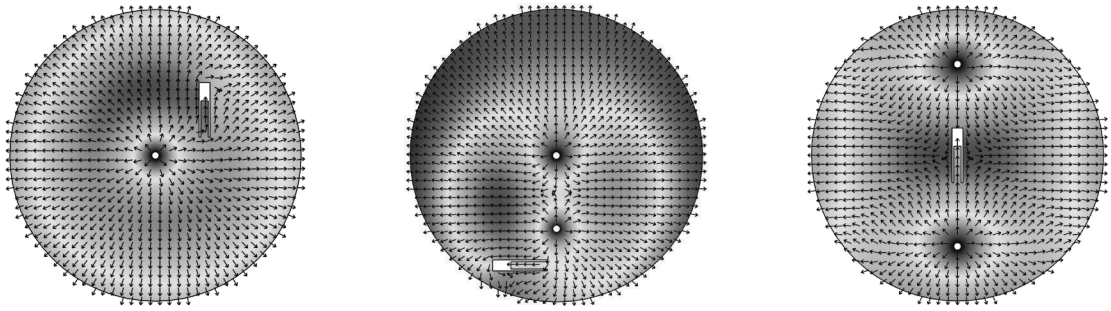

(a) (b) (c)

Figure 8: Pressure distribution and intensity flow in a free field with (a) one and (b) and (c) two sources.

Table 1: Sound intensity measured in an enclosure using the SIAF-prototype.

f/Hz	100	125	250	500
I_{SIAF}/Wm^{-2} without control	−0.043	−0.018	−0.002	−0.004
I_{SIAF}/Wm^{-2} with control	+0.056	+0.048	+0.018	+0.006
I_{Conv}/Wm^{-2} without control	+0.536	+0.107	+0.292	+0.348

relevant error types, the mean deviation in the analyzed frequency band, calculated as

$$\Delta\bar{I} := 10\log_{10}\left(\frac{1}{N_f}\sum_{i=1}^{N_f}\frac{10^{|\Delta I_i|/10}}{10^{-12}\,\mathrm{Wm}^{-2}}\right), \tag{11}$$

where N_f (representing the number of analyzed frequencies) could be reduced from 3.24 dB down to 0.61 dB. The maximum deviation was reduced from 4.2 dB down to −1.5 dB. A minimum deviation of 0.1 dB was found at 200 Hz after correction. The results prove that the SIAF prototype can be calibrated successfully under well-defined boundary conditions. For practical use, however, a calibrator that can easily be attached and coupled to a well-defined sound source (e.g., a pistonphone) would be required.

The experimental setup shown in Figure 5(b) was a simple example of a sound source that is located directly in front of the entrance of the tube. To study the SIAF concept for other arrangements, time-harmonic finite element simulations ($f = 300$ Hz) were carried out in two dimensions using free field conditions for the outer boundary of the analyzed area. It was found, that a SIAF placed in a certain distance to the surface of the source would again act as a local absorber that changes the direction of the energy flow as motivated by Figure 8(a). If two uncorrelated sources are present, and the SIAF would again not be collocated to one of these sources, the time average of the local intensity in longitudinal probe direction would be measured, as shown in Figure 8(b). This quantity would be determined by the sound field generated by these interfering sources. If the SIAF is placed between two sources with equal strength, as illustrated by Figure 8(c), the uni-directional intensity component of the source facing the open end of the sound tube would be measured.

Using the arrangement consisting of loudspeaker, accelerometer, and SIAF, compare with Figure 5(b), the prototype was also tested in a typical lab. The reverberation time of this room varies between 0.85 second at 125 Hz and 0.5 second at 400 Hz. The arithmetic mean in the frequency band between 100 Hz and 5 kHz is given by 0.64 second and corresponds to values desired for rooms of medium size (250 m^3–5000 m^3), see [19]. In this situation, a positive sound intensity was measured for every tested frequency, if active noise control based on wave separation in time domain was applied. The data shown in Table 1 indicates that a SIAF can also be used to detect acoustic hot spots in weakly damped interiors as proposed in [7].

The sound intensities that were measured directly in front of the loudspeaker using the conventional sound intensity probe—without the surrounding sound tube and without active control—are also listed in Table 1. The comparison of the results proves that the SIAF was indeed capable of detecting the loudspeaker as an acoustic source. In contrast to the calibration test that was performed under idealized conditions, the magnitudes of I_{SIAF} (with control) and I_{Conv} cannot be compared, because the first quantifies the energy transport of travelling plane waves that are absorbed inside the SIAF, whereas the second quantifies the circulation of energy in the (partly active and partly reactive) near field of an acoustic source that acts in a standing wave field.

It is obvious that it is more sophisticated to calculate the plane wave error for sound fields excited by more complicated sources than used in the calibration tests. Nevertheless, to identify a sound source by application of the SIAF approach that works under conditions in which conventional methods cannot be used, it is sufficient to detect a positive energy flow, even if the absolute values are not equal to values that can be measured with sensors of top-level quality.

4. SUMMARY AND OUTLOOK

The functioning principle as well as a prototype of a new sound intensity probe was presented. It was found that a free field can be realized inside this probe by active noise control, if a microphone pair in combination with a wave separation approach is used to determine the reflected wave components. The FxLMS algorithm was used for the signal control task using an accelerometer as a nonacoustic reference sensor. This approach will be sufficient, if access to a signal which is linearly related to the disturbance is given (e.g., in an acoustic test center or during acoustic ground tests of new aircrafts). It was shown that a sound intensity probe with an active free field can be calibrated successfully inside an anechoic chamber, if the finite difference approximation errors that appear during numerical calculation of the pressure gradient based on a two microphone technique, the near field error, and the deviations between plane wave propagation in one dimension and spherical wave propagation in three dimensions are taken into account. But, at this stage of development, the accuracy of the SIAF is of course not as high as the accuracy of well-established conventional probes. It was also found that, because of the active-free field inside the probe, a SIAF is capable of detecting an acoustic source inside standing wave fields that typically appear in weakly damped interiors. Future research will be focussed on the development of a calibration procedure that allows calibration outside an anechoic chamber. To be independent of a reference signal that is well correlated to the disturbance, the application of a stable feedback controller is intended. Furthermore, it is planned to redesign the shape of the open end of the SIAF in order to smooth the change of impedance along the inlet of the probe by conical or exponential horns.

REFERENCES

[1] J. J. Christensen and J. Hald, "Beamforming," *Technical Review 1*, pp. 1–35, Brüel & Kjaer, Naerum, Denmark, 2004.

[2] J. Hald, "STSF—a unique technique for scan-based near-field acoustic holography without restrictions on coherence," *Technical Review 1*, pp. 1–50, Brüel & Kjaer, Naerum, Denmark, 1989.

[3] J. D. Maynard, E. G. Williams, and Y. Lee, "Nearfield acoustic holography: I. Theory of generalized holography and the development of NAH," *The Journal of the Acoustical Society of America*, vol. 78, no. 4, pp. 395–1413, 1985.

[4] K. R. Holland and P. A. Nelson, "Sound source characterization: the focussed beamformer vs the inverse method," in *Proceedings of the 11th International Congress on Sound and Vibration (ICSV '04)*, pp. 1913–1920, St. Petersburg, Russia, July 2004.

[5] J. Drenckhan and D. Sachau, "Identification of sound sources using inverse FEM," in *Proceeding of the 10th International Congress on Sound and Vibration*, pp. 1913–1920, Stockholm, Sweden, July 2003.

[6] T. Kletschkowski and D. Sachau, "Noise source identification using a sound intensity probe with active free-field," in *Proceedings of 8th Conference on Active Noise and Vibration Control Methods*, Krakow-Krasiczyn, Poland, June 2007.

[7] D. Sachau, J. Drenckhan, and I. Schäfer, "Schallintensitätsdetektor sowie Verfahren zum Messen der Schallintensität," 2004, Patent Application No. 10 2004 009 644.9, Germany.

[8] H. Freienstein and D. Guicking, "Experimentelle Untersuchung von linearen Lautsprecheranordnungen als aktive Absorber in einem Kanal," in *Fortschritte der Akustik (DAGA '96)*, pp. 112–113, Bonn, Germany, February 1996.

[9] M. Utsumi, "Reduction of noise transmission in a duct by termination impedance control of a sidebranch resonator," *Journal of Vibration and Acoustics*, vol. 123, no. 3, pp. 289–296, 2001.

[10] "Acoustics—determination of sound absorption coefficient and impedance in impedance tubes—part 2: transfer-function method," 2001, EN ISO 10534-2.

[11] M. J. Crocker and J. P. Arenas, "Fundamentals of direct measurement of sound intensity an practical applications," *Acoustical Physics*, vol. 49, no. 2, pp. 163–175, 2003.

[12] D. Guicking and K. Karcher, "Active impedance for one-dimensional sound," *Journal of Vibration, Acoustics, Stress, and Reliability in Design*, vol. 106, pp. 393–396, 1984.

[13] M. S. Kou and D. R. Morgan, *Active Noise Control Systems: Algorithms and DSP Implementations*, John Wiley & Sons, New York, NY, USA, 1996.

[14] F. Jacobsen and H.-E. de Bree, "A comparison of two different sound intensity measurement principles," *The Journal of the Acoustical Society of America*, vol. 118, no. 3, pp. 1510–1517, 2005.

[15] S. Baker, "An acoustic intensity metes," *The Journal of the Acoustical Society of America*, vol. 27, no. 2, pp. 269–273, 1955.

[16] M. Hamann, *Ein Beitrag zur Realisierung eines Schallintensitätsmessverfahrens*, Ph.D. dissertation, University of Hannover, Hannover, Germany, 1980.

[17] Datasheet PU sound probe. Microflown technologies, Zevenaar, The Netherlands, 2006.

[18] F. X. Pinget, *Aktive Erzeugung der Sommerfeld'schen Randbedingungen unter Verwendung eines neuen Schnellesensors*, Diploma-Thesis, Helmut-Schmidt-University/University of the Federal Armed Forces Hamburg, Hamburg, Germany, 2005.

[19] "Acoustical quality in small to medium-sized rooms," 2004, DIN 18041.